

Prospects of Jet Tomography Using Hard Processes inside a Soft Medium

Thorsten Renk*

*Department of Physics, P.O. Box 35 FI-40014 University of Jyväskylä, Finland and
Helsinki Institute of Physics, P.O. Box 64 FI-00014, University of Helsinki, Finland*

E-mail: trenk@phys.jyu.fi

Kari J. Eskola

*Department of Physics, P.O. Box 35 FI-40014 University of Jyväskylä, Finland and
Helsinki Institute of Physics, P.O. Box 64 FI-00014, University of Helsinki, Finland*

E-mail: kari.eskola@phys.jyu.fi

The term 'tomography' is commonly applied to the idea of studying properties of a medium by the modifications this medium induces to a known probe propagating through it. In the context of ultrarelativistic heavy-ion collisions, rare high transverse momentum (p_T) processes taking place alongside soft bulk-matter production can be viewed as a tomographic probe as long as the energy scales are such that the modification of high p_T processes can be dominantly ascribed to interactions with the medium during the propagation of partons. Various high p_T observables have been suggested for tomography, among them hard single hadron suppression, dihadron correlations and γ -hadron correlations. In this paper, we present a model study of a number of different observables within the same calculational framework to assess the sensitivity of the observables to different properties of the medium and discuss the prospects of obtaining tomographic information.

High- p_T physics at LHC

March 23-27, 2007

University of Jyväskylä, Jyväskylä, Finland

*Speaker.

1. Introduction

The expression 'jet tomography' is often used to describe the analysis of hard perturbative Quantum Chromodynamics (pQCD) processes taking place inside the soft matter created in an ultrarelativistic heavy-ion collision. Such processes, which are well understood in p-p collisions, can be viewed as a known probe as they take place before any formation scale of a soft medium. Thus, only the subsequent propagation of partons through the soft medium (and possibly hadronization, although at sufficiently high p_T the hadron formation length is larger than the medium extension) is sensitive to interactions with the medium. Hence, any modification of hard processes embedded in a medium potentially carries tomographic information about the medium properties.

In particular the experimental focus is on the nuclear suppression of hard hadrons in A-A collisions compared with the scaled baseline from p-p collisions, which is expected due to interactions of a hard parton with the soft medium (see e.g. [1]). However, the nuclear suppression factor

$$R_{AA}(p_T, y) = \frac{d^2 N^{AA}/dp_T dy}{T_{AA}(\mathbf{b}) d^2 \sigma^{NN}/dp_T dy}. \quad (1.1)$$

is a rather integral quantity, arising in model calculations from a convolution of the hard pQCD vacuum cross section $d\sigma_{vac}^{AA \rightarrow f+X}$ for the production of a parton f , the energy loss probability $P_f(\Delta E)$ given the vertex position and path through the medium and the vacuum fragmentation function $D_{f \rightarrow h}^{vac}(z, \mu_F^2)$, as schematically expressed

$$d\sigma_{med}^{AA \rightarrow h+X} = \sum_f d\sigma_{vac}^{AA \rightarrow f+X} \otimes P_f(\Delta E) \otimes D_{f \rightarrow h}^{vac}(z, \mu_F^2), \quad (1.2)$$

where

$$d\sigma_{vac}^{AA \rightarrow f+X} = \sum_{ijk} f_{i/A}(x_1, Q^2) \otimes f_{j/A}(x_2, Q^2) \otimes \hat{\sigma}_{ij \rightarrow f+k}. \quad (1.3)$$

Here, $f_{i/A}(x, Q^2)$ denotes the nuclear parton distribution function which depends on the parton momentum fraction x and the hard momentum scale Q^2 and $\hat{\sigma}_{ij \rightarrow f+k}$ is the partonic pQCD cross section.

Eq. (1.2) has to be properly averaged over all possible vertices distributed according to the nuclear overlap T_{AA} and all possible paths through the medium. In [2] we have argued that one can factorize this spatial averaging from the momentum space formulation Eq. (1.2) and thus define the geometry-averaged energy loss probability $\langle P(\Delta E, E) \rangle_{T_{AA}}$. R_{AA} can thus be viewed as providing constraints for the form of $\langle P(\Delta E, E) \rangle_{T_{AA}}$.

2. Calculational framework

Any model for medium modifications of a hard process must contain three major ingredients: The hard pQCD process, the bulk matter evolution for which we either use a hydrodynamic [3] or a parametrized evolution model [4] and the energy loss probability distribution given a hard parton path through the soft medium [5].

The primary hard process is calculated in leading order pQCD under the assumption that the transverse momentum scale is large enough so that hadronization takes place outside the medium

and that the produced leading hadron can be assumed to be collinear with its parent parton. The calculation, when supplemented by a K-factor, agrees well with hard hadron production measured in p-p collisions. In particular, the AKK set of fragmentation functions [6] also gives a satisfactory description of proton production whereas the older KKP set [7] does not. Explicit expressions for the hard process calculation can be found e.g. in [8].

The interaction of the hard parton with the soft medium is calculated using the radiative energy loss formalism of [5]. If we call the angle between outgoing parton and the reaction plane ϕ , the path of a given parton through the medium $\xi(\tau)$ is specified by (\mathbf{r}_0, ϕ) and we can compute the energy loss probability $P(\Delta E)_{path}$ for this path. We do this by evaluating the line integrals

$$\omega_c(\mathbf{r}_0, \phi) = \int_0^\infty d\xi \xi \hat{q}(\xi) \quad \text{and} \quad \langle \hat{q}L \rangle(\mathbf{r}_0, \phi) = \int_0^\infty d\xi \hat{q}(\xi) \quad (2.1)$$

along the path where we assume the relation

$$\hat{q}(\xi) = K \cdot 2 \cdot \varepsilon^{3/4}(\xi) (\cosh \rho - \sinh \rho \cos \alpha) \quad (2.2)$$

between the local transport coefficient $\hat{q}(\xi)$ (specifying the quenching power of the medium), the energy density ε and the local flow rapidity ρ with angle α between flow and parton trajectory [9, 10]. Here ω_c is the characteristic gluon frequency, setting the scale of the energy loss probability distribution, and $\langle \hat{q}L \rangle$ is a measure of the path-length weighted by the local quenching power. We view the parameter K as a tool to account for the uncertainty in the selection of α_s and possible non-perturbative effects increasing the quenching power of the medium (see discussion in [8]) and adjust it such that pionic R_{AA} for central Au-Au collisions is described. Using the numerical results of [5], we obtain $P(\Delta E; \omega_c, R)_{path}$ for ω_c and $R = 2\omega_c^2 / \langle \hat{q}L \rangle$ as a function of jet production vertex and the angle ϕ .

The information about the soft medium is contained in the local energy density $\varepsilon(\xi)$ and the flow rapidity $\rho(\xi)$. These parameters are obtained from dynamical evolution models which are tuned to describe a large body of bulk matter observables [3, 4]. Details of the evolution models including contour plots of their time evolution can be found in [8]. In the following, we mainly illustrate three scenarios: A hydrodynamical evolution of matter ('Hydrodynamics'), the best fit to soft hadronic p_T spectra and HBT correlation data of the parametrized evolution model ('Box density') and the hydrodynamical model under the assumption that only the partonic evolution phase leads to energy loss ('Black core'). Since in all models R_{AA} for central Au-Au collisions is described by construction via a fit of K , the latter model implies that K takes large values and the evolution exhibits a very black interior region and a dilute hadronic halo which does not induce energy loss at all, quite different from the other models.

3. Single Hadron Suppression

Since R_{AA} does not contain any spatial information, the production vertices of hard partons and their path through the medium have to be averaged out. Hard vertices (x_0, y_0) are distributed according to a probability density

$$P(x_0, y_0) = \frac{T_A(\mathbf{r}_0 + \mathbf{b}/2) T_A(\mathbf{r}_0 - \mathbf{b}/2)}{T_{AA}(\mathbf{b})}, \quad (3.1)$$

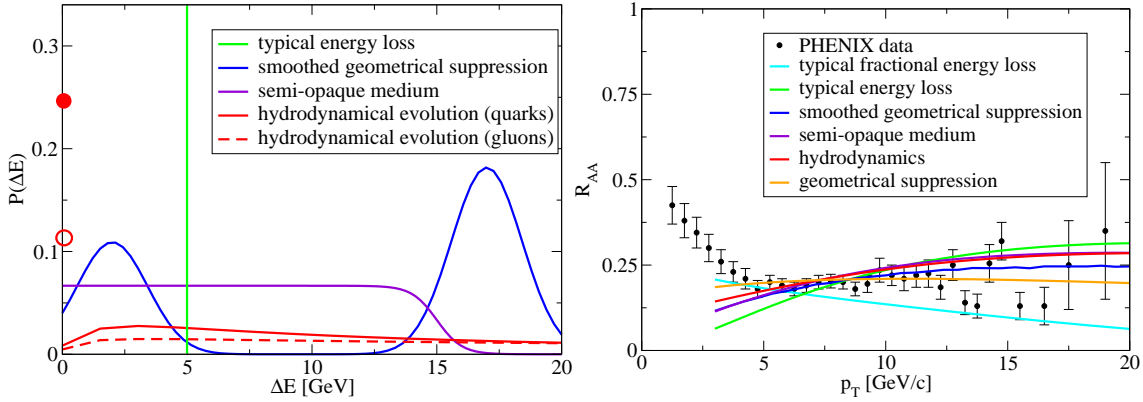


Figure 1: Left panel: Trial energy loss distributions $\langle P(\Delta E) \rangle_{T_{AA}}$ for various scenarios of jet energy loss in the medium (see text and [2] for details). Right panel: R_{AA} as calculated from the trial distributions shown on the left hand side.

where \mathbf{b} is the impact parameter. The thickness function is given by the nuclear density $\rho_A(\mathbf{r}, z)$ as $T_A(\mathbf{r}) = \int dz \rho_A(\mathbf{r}, z)$. Hence, given the energy loss probability distribution $P_f(\Delta E)_{path}$ for a given path through the medium, we obtain

$$\langle P_f(\Delta E, E) \rangle_{T_{AA}} = \frac{1}{2\pi} \int_0^{2\pi} d\phi \int_{-\infty}^{\infty} dx_0 \int_{-\infty}^{\infty} dy_0 P(x_0, y_0) P_f(\Delta E)_{path}. \quad (3.2)$$

Before we proceed to calculate this quantity, let us illustrate the sensitivity of R_{AA} to details of $\langle P_f(\Delta E) \rangle_{T_{AA}}$ (and hence the potential for tomographic information) by inserting trial distributions into the folding integral Eq. (1.2). These trial distributions are shown in Fig. 1, left panel, the resulting R_{AA} is shown in the right panel and compared with the PHENIX data for pions [11] (see also [2] for details).

It is apparent from the figure that despite strong differences in the functional form of $\langle P(\Delta E) \rangle_{T_{AA}}$, all distributions describe the measured R_{AA} reasonably well above some minimum p_T . The notable exception is the case of a constant fractional energy loss in which R_{AA} drops as a function of p_T , which does not seem to capture the overall trend well. It has to be concluded that R_{AA} does not exhibit great tomographic capability beyond a single overall energy loss scale (the numerical value of which moreover is different for each model). This may explain why different calculations extract rather different quenching properties of the medium from fits to R_{AA} .

However, while the curves are reasonably similar over the kinematic range shown here, they do show differences in details which unfortunately cannot be resolved within the current data precision. Thus, there is some reason to suspect that either increased experimental statistics or a larger accessible kinematic range may provide more stringent constraints for the energy loss distribution.

In Fig. 2 left panel we show the calculated R_{AA} using the procedure outlined above to determine $\langle P(\Delta E) \rangle_{T_{AA}}$ instead of a trial ansatz. Once K is adjusted, the result does not exhibit strong sensitivity to the underlying medium evolution model (we do not show the results for all different medium evolutions here as the curves are difficult to distinguish), again confirming that R_{AA} has very limited tomographic capability in the RHIC kinematic range.

If the AKK fragmentations [6] are used for computation for which the baseline process of

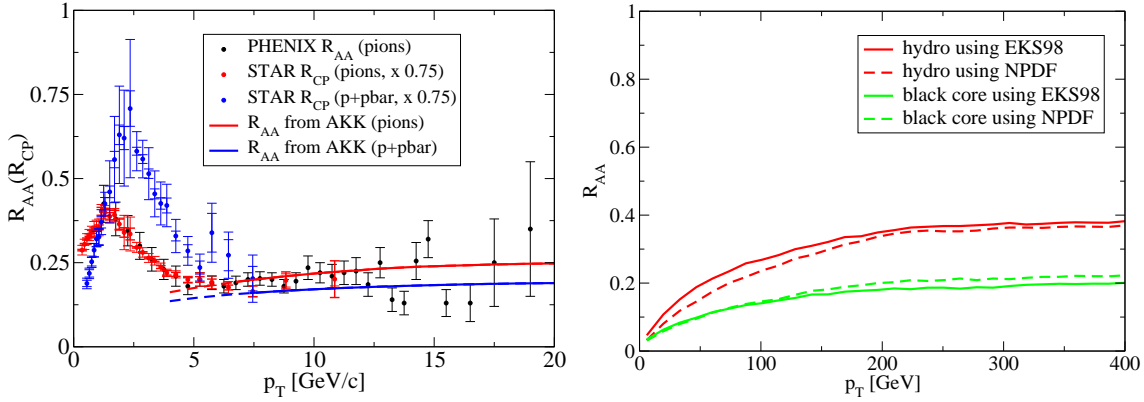


Figure 2: Left panel: R_{AA} for pions and protons as compared to the measured R_{AA} (R_{CP}) data [11, 12] for RHIC conditions Right panel: Model predictions for R_{AA} at the LHC based on two scenarios which describe the data at RHIC [14].

proton production in p-p collisions is roughly under control (in detail, AKK seems to overpredict the process by about a factor 2), the calculation of R_{AA} for both pions and protons agrees well with the data [13]. This is not a trivial result, as in the AKK fragmentation scenario proton production is gluon-dominated whereas pion production is not, hence the difference between pion and proton production should reflect the different energy loss properties of quarks and gluons. In the calculation as presented here, the rather small difference between proton and pion suppression is caused by the fact that gluon suppression is already in a saturated regime — increasing the quenching power of the medium further induces only a small change in the gluonic R_{AA} [13].

In Fig. 2, right panel we show the extrapolation of the p_T dependence of R_{AA} to LHC energies based on the hydrodynamical scenarios which describe the data at RHIC [3, 14]. While there is some uncertainty associated with the extrapolation of the nuclear parton distribution function (NPDF [15] vs. EKS98 [16]), this is a small effect, and it becomes indeed apparent that with the extended kinematic lever-arm of LHC the different properties of the two scenarios (dense core and dilute halo vs. more evenly distributed quenching power) can clearly be distinguished. The results here differ from a previous calculation presented in [17]. The improvement of the present calculation over the previous work is chiefly in the use of a dynamically evolving soft medium instead of a static cylinder ansatz and in using Eq. (3.1) for the primary vertex distribution as compared to a homogeneous distribution.

Let us illustrate the differences induced by the spatial distribution of the quenching power by studying the geometry of single hadron suppression directly in the model. In Fig. 3 we show the probability density of finding the primary pQCD vertex leading to an observed hadron above 8 GeV in p_T . It is evident (and quite expected) that emission occurs predominantly close to the near side surface of the medium. However, the degree to which surface emission is realized is quite different in all three models. Clearly, the strong suppression from the core region of the black core scenario repels the distribution much more from the center than the more even distribution of the other two scenarios. Thus, surface emission is not a property of a particular energy loss formalism, but arises from the interplay of energy loss formalism with the underlying geometry and evolution of the soft medium.

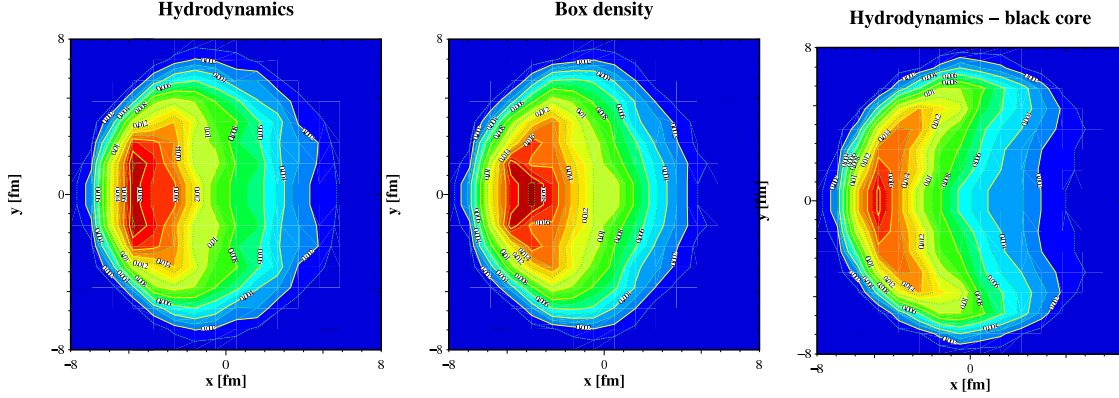


Figure 3: Probability density for finding a hard vertex in the transverse plane in 200 AGeV Au-Au collisions leading to an observed hadron above 8 GeV transverse momentum, shown for three different medium evolution scenarios (see text). In all cases, the hard hadron propagation defines the $-x$ direction. All contour intervals are linear.

4. Dihadron suppression

We can make use of the sensitivity of the vertex distribution of single hadron suppression to the medium evolution by considering dihadron suppression. In a back-to-back event, the second hadron propagation path is not averaged over the initial overlap Eq. (3.1) but over a conditional probability distribution given a valid trigger, i.e. over the distribution shown in Fig. 3 (which is quite different from the overlap). Thus, even if two model evolutions lead to identical R_{AA} , this does not mean that they would produce the same dihadron correlation pattern. We call this conditional probability distribution given a high- p_T near-side trigger in the following $\langle P(\Delta E) \rangle_{Tr}$ and investigate its capability to obtain tomographical information.

For computational purposes, we employ a Monte-Carlo (MC) simulation of the experimental trigger condition, followed by the simulation of the away-side parton intrinsic- k_T smearing, propagation, energy loss and fragmentation. The procedure is described in detail in [8].

In Fig. 4 we compare the yield per trigger on the near and away side for different medium models with the data obtained by the STAR collaboration [18, 19]. Within errors, the near side yield per trigger is described by all the models well. There is no significant disagreement among the models. The model calculations appear significantly more different if we consider the away side yield. Here, results for the 4-6 GeV momentum bin differ by almost a factor two. However, none of the model calculations describes the data in this bin. This is in fact not at all surprising as below 5 GeV the inclusive single hadron transverse momentum spectra are not dominated by pQCD fragmentation and energy losses but, rather, by hydrodynamics possibly supplemented with recombination [20, 21] type phenomena. For this reason, the ratio R_{AA} at $p_T < 5$ GeV cannot be expected to be described by pQCD fragmentation and energy losses, either.

This is clearly unfortunate, as the model results are considerably closer to the experimental result in the 6+ momentum bin on the away side and hence our ability to discriminate between different models is reduced. Since at this large transverse momenta the pQCD fragmentation + energy losses dominate the single hadron spectrum, we expect that the model is able to give a valid description of the relevant physics in this bin: Not only is R_{AA} well described by the data, but also

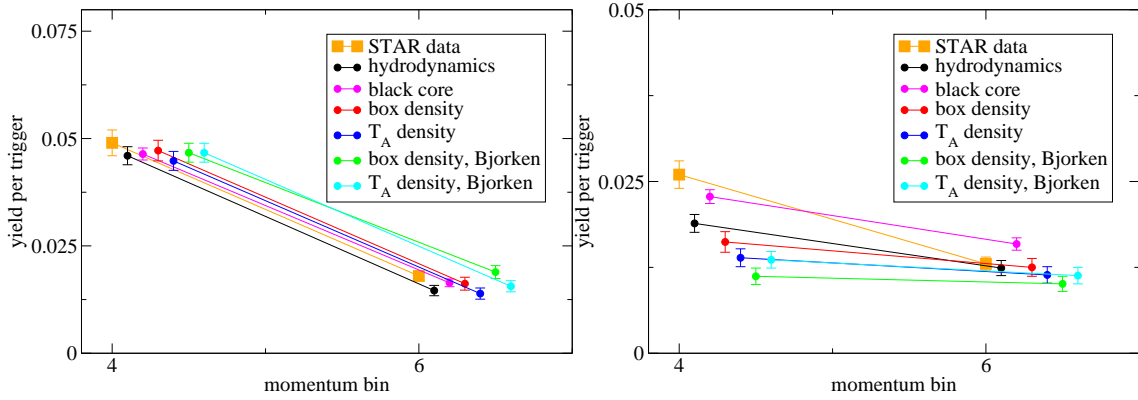


Figure 4: Yield per trigger on the near side (left panel) and away side (right panel) of hadrons in the 4-6 GeV and 6+ GeV momentum bin associated with a trigger in the range $8 \text{ GeV} < p_T < 15 \text{ GeV}$ for the different models of spacetime evolution as compared with the STAR data [18, 19]. The individual data points have been spread artificially along the x axis for clarity of presentation.

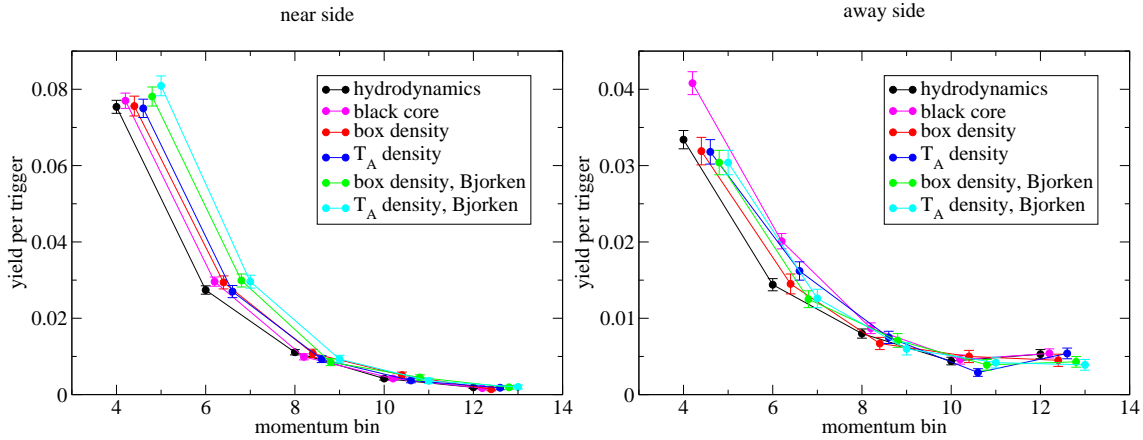


Figure 5: Yield per trigger on the near side (left panel) and away side (right panel) of hadrons in the 4-6 GeV and 6+ GeV momentum bin associated with a trigger in the range $12 \text{ GeV} < p_T < 20 \text{ GeV}$ for the different models of spacetime evolution. The individual data points have been spread artificially along the x axis for clarity of presentation.

the contribution of recombination processes to the yield is expected to be small [20]. Thus, as it stands, only the black core scenario can be ruled out by the data, the box density with Bjorken expansion seems strongly disfavoured but still marginally acceptable.

Thus, as it stands, the kinematic window to study dihadron correlations in a perturbatively calculable region is not enough to exploit the difference between $\langle P(\Delta E) \rangle_{Tr}$ and $\langle P(\Delta E) \rangle_{RAA}$ and thus to obtain detailed tomographic information. However, the situation may improve for an increased kinematical window in the region where pQCD + fragmentation can be applied. In order to test this, we redo the MC simulation with trigger hadrons in the range between 12 and 20 GeV.

The distribution after fragmentation into hadrons in bins of 2 GeV width in the perturbative region is shown in Fig. 5 for the near side (left panel) and away side (right panel). It is again apparent that within errors all models agree in the expected near side yield. The momentum spectrum

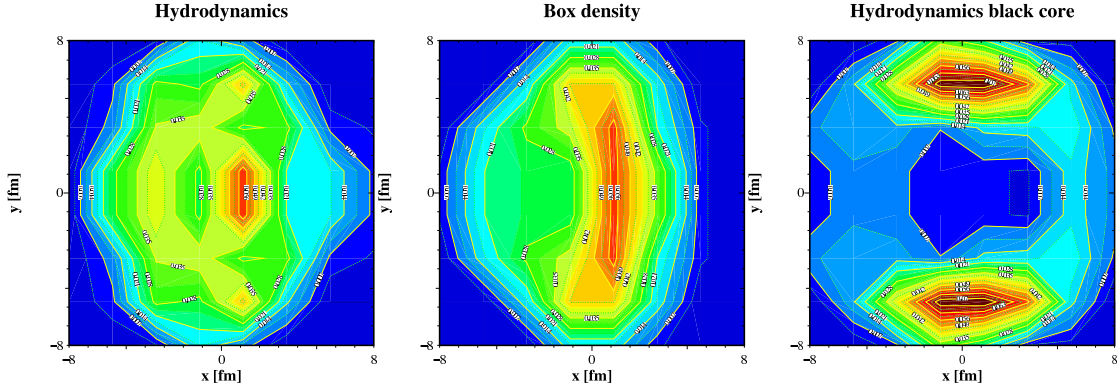


Figure 6: Probability density for finding a hard vertex in the transverse plane in 200 AGeV Au-Au collisions leading to an event with both an observed near side hadron above $p_T = 8$ GeV (defining the $-x$ direction) and an away side hadron with $p_T > 4$ GeV for three different medium evolutions (see text). All contour intervals are linear.

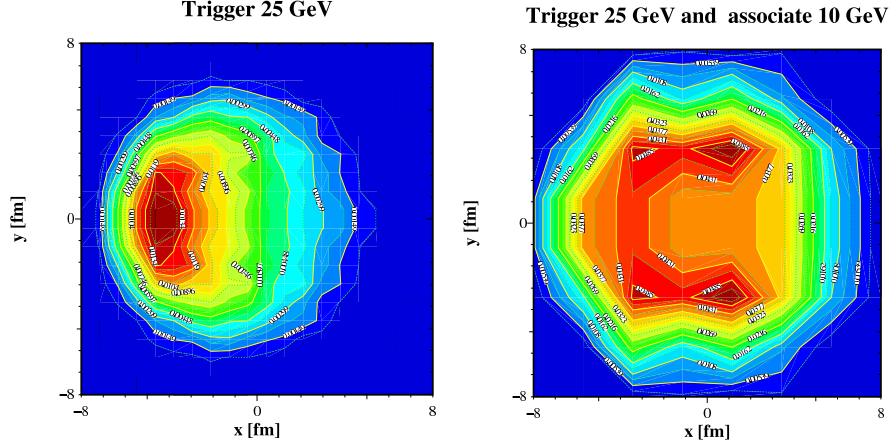


Figure 7: Left panel: Probability density for finding a hard vertex in the transverse plane in 5.5 ATeV Pb-Pb collisions leading to a near side hadron with $p_T > 25$ GeV propagating into the $-x$ direction for the LHC hydrodynamical model prediction. Right: Probability density requiring in addition an associated away side hadron with $p_T > 10$ GeV momentum. All contour intervals are linear.

of the away side exhibits considerably more structure. Several of the scenarios can now be clearly told apart in bins in the perturbative region. For example the T_A and the box density (which have virtually identical $\langle P(\Delta E) \rangle_{T_{AA}}$) show almost a factor two difference in the 10-12 GeV momentum bin. As we have seen above in the case of the LHC extrapolation, is evident again from the analysis that having a larger lever-arm in momentum is needed to get access to tomographic information.

Finally, let us discuss the geometry of dihadron suppression. In Fig. 6 we show the probability density of finding a hard vertex leading to a high p_T near side trigger and a correlated associated hard away side hadron. Here, clear differences between tangential emission in the case of a dense core and production across the whole volume become apparent.

In Fig. 7 we also show the geometry of single hadron and dihadron suppression for LHC conditions in central Pb-Pb collisions. For a 25 GeV trigger hadron, we expect some degree of surface emission (note that the dihadron production distribution is somewhat repelled from the

center) but no strong tangential emission.

5. A simple model

As we have seen, quite a general class of models predict a small rise of R_{AA} with p_T at RHIC and a more pronounced one at LHC. Assuming RHIC kinematics, R_{AA} is rather insensitive to details of the energy loss probability distributions, at LHC the sensitivity is considerably enhanced. Likewise, dihadron correlations become more sensitive to the medium density distribution if the kinematic range is increased. In the following, let us try to illustrate that all these observations can be understood from simple considerations.

Quite generally, energy loss probability distributions can be decomposed as

$$\langle P(\Delta E) \rangle_{T_{AA}(Tr)} = T \delta(\Delta E) + S \cdot P(\Delta E) + A \cdot \delta(\Delta E - E) \quad (5.1)$$

where T is a transmission term describing a parton penetrating through the medium without energy loss, S is a shift term which characterizes partons emerging from the medium after a finite energy loss and A is an absorption term describing partons which have been shifted in energy so much that they become part of the soft medium.

Let us now assume a power law for the parton spectrum at RHIC and LHC $\sim 1/p_T^n$ with $n_{RHIC} > n_{LHC}$. Energy loss ΔE then changes this spectrum to $1/(p_T + \Delta E)^n$, thus R_{AA} in this simple model can be obtained from

$$R_{AA} \approx \int d\Delta E \langle P(\Delta E) \rangle_{T_{AA}} 1 / \left(1 + \frac{\Delta E}{p_T} \right)^n$$

It is evident from the expression that R_{AA} at given p_T is equal to the transmission term T plus a contribution which is proportional to the integral of $\langle P(\Delta E) \rangle_{T_{AA}}$ from zero up to the energy scale E_{max} of the parton, *seen through the filter* of the steeply falling spectrum. R_{AA} grows with p_T since E_{max} grows linearly with p_T . However, at RHIC conditions the characteristic scale ω_c of the energy loss probability distribution is far above E_{max} , thus the growth is slow and R_{AA} is dominated by T , rendering it almost a constant. Since tomographic information is mainly contained in the shift term S , the apparent insensitivity of R_{AA} to assumptions about the medium can be understood.

This is very different at LHC where $E_{max} \sim \omega_c$ (since E_{max} grows linear with p_T but ω_c grows with the entropy density and hence much slower) and a pronounced contribution of the shift term can be probed. Here, a rise of R_{AA} with p_T is expected, along with a greater tomographic sensitivity.

6. Conclusions

We have investigated the capability of single and dihadron suppression to provide tomographic information about the soft medium created in ultrarelativistic heavy-ion collisions. We have argued that at RHIC kinematics, the nuclear suppression factor R_{AA} is not very sensitive to the medium evolution. While dihadron suppression, due to its different geometrical averaging, exhibits in principle more sensitivity to medium properties, unfortunately the present data situation allows only to rule out a very pronounced difference between a strongly absorbing core and a dilute halo. This

insensitivity can be traced back to the fact that ω_c , the intrinsic scale for energy loss is much higher than E_{max} , the accessible parton energy at RHIC.

However, when going to LHC energies, this condition no longer holds. R_{AA} becomes dominated by partons being shifted in energy, and tomographic information can be recovered even from the p_T dependence of R_{AA} . Dihadron correlations and other measurements, such as γ -hadron correlations [2] which provide a monochromatic source of hard quarks in the medium or R_{AA} vs. reaction plane [22], which allows for a systematic variation of in-medium pathlength, may provide additional information such that a multi-pronged approach to jet tomography finally becomes feasible.

References

- [1] M. Gyulassy, P. Levai and I. Vitev, Phys. Lett. B **538** (2002) 282; E. Wang and X. N. Wang, Phys. Rev. Lett. **89** (2002) 162301; C. A. Salgado and U. A. Wiedemann, Phys. Rev. Lett. **89** (2002) 092303; G. G. Barnafoldi, P. Levai, G. Papp, G. I. Fai and M. Gyulassy, Eur. Phys. J. C **33** (2004) S609; S. Wicks, W. Horowitz, M. Djordjevic and M. Gyulassy, Nucl. Phys. A **784** (2007) 426.
- [2] T. Renk, Phys. Rev. C **74** (2006) 034906.
- [3] K. J. Eskola, H. Honkanen, H. Niemi, P. V. Ruuskanen and S. S. Räsänen, Phys. Rev. C **72** (2005) 044904.
- [4] T. Renk, Phys. Rev. C **70** (2004) 021903.
- [5] C. A. Salgado and U. A. Wiedemann, Phys. Rev. D **68**, (2003) 014008.
- [6] S. Albino, B. A. Kniehl and G. Kramer, Nucl. Phys. B **725** (2005) 181.
- [7] B. A. Kniehl, G. Kramer and B. Potter, Nucl. Phys. B **582**, (2000) 514.
- [8] T. Renk and K. J. Eskola, Phys. Rev. C **75** (2007) 054910.
- [9] R. Baier, A. H. Mueller and D. Schiff, nucl-th/0612068.
- [10] H. Liu, K. Rajagopal and U. A. Wiedemann, JHEP **0703**, 066 (2007).
- [11] M. Shimomura [PHENIX Collaboration], nucl-ex/0510023.
- [12] B. I. Abelev *et al.* [STAR Collaboration], Phys. Rev. Lett. **97** (2006) 152301.
- [13] T. Renk and K. J. Eskola, hep-ph/0702096.
- [14] T. Renk and K. J. Eskola, 0705.1881 [hep-ph].
- [15] M. Hirai, S. Kumano and T. H. Nagai, Phys. Rev. C **70**, (2004) 044905.
- [16] K. J. Eskola, V. J. Kolhinen and C. A. Salgado, Eur. Phys. J. C **9** (1999) 61.
- [17] K. J. Eskola, H. Honkanen, C. A. Salgado and U. A. Wiedemann, Nucl. Phys. A **747** (2005) 511.
- [18] D. Magestro [STAR Collaboration], nucl-ex/0510002; talk Quark Matter 2005.
- [19] J. Adams *et al.* [STAR Collaboration], nucl-ex/0604018.
- [20] R. J. Fries, B. Muller, C. Nonaka and S. A. Bass, Phys. Rev. C **68** (2003) 044902.
- [21] R. C. Hwa and C. B. Yang, Phys. Rev. C **70** (2004) 024905.
- [22] T. Renk, J. Ruppert, C. Nonaka and S. A. Bass, Phys. Rev. C **75** (2007) 031902.